Materials Research. 2019; 22(5): e20190305
DOI: http://dx.doi.org/10.1590/1980-5373-MR-2019-0305

Nb-Al Binary System: Reevaluation of the Solubility Limits of the (Nb), Nb_3Al, Nb_2Al and $NbAl_3$ Phases at High Temperatures

***Antonio Augusto Araujo Pinto da Silva*[a]*, *Gilberto Carvalho Coelho*[b], *Carlos Angelo Nunes*[b], *Jean Marc Fiorani*[c], *Nicolas David*[c], *Michel Vilasi*[c]**

[a]*Instituto de Engenharia Mecânica - IEM, Universidade Federal de Itajubá – UNIFEI, Avenida BPS, 1303, 37500-903, Itajubá, MG, Brasil*
[b]*Escola de Engenharia de Lorena - EEL, Universidade de São Paulo – USP, Estrada Municipal do Campinho, 12600-000, Lorena, SP, Brasil*
[c]*Institut Jean Lamour - IJL, Université de Lorraine – UL, BP 70239, 54506, Vandœuvre-lès-Nancy, France*

Received: April 24, 2019; Revised: July 26, 2019; Accepted: August 27, 2019.

In this work a re-investigation of the solubility limits of the (Nb), Nb_3Al, Nb_2Al and the Nb-rich side of the $NbAl_3$ phases on the Nb-Al system is presented. Alloys in the binary fields ((Nb)+Nb_3Al, Nb_3Al+Nb_2Al and Nb_2Al+$NbAl_3$) were arc-melted, and then equilibrated at 1000, 1200 and 1400 °C. The phases were confirmed via X-ray powder diffractometry, and their compositions were determined via EPMA measurements. The results showed agreement with the literature concerning the solubility limits of (Nb), Nb_3Al and $NbAl_3$ phases, while important differences in the values were found for the Nb_2Al phase. In addition, the lattice parameters of the Nb_2Al phase were determined via Rietveld refinement. This new set of more accurate experimental information indicates that a thermodynamic reassessment is necessary to precisely describe this system.

Keywords: *intermetallics, phase diagrams, Nb-Al system.*

1. Introduction

Accurate description of binaries and ternaries phase diagrams is of fundamental importance for the development of thermodynamic databases, useful to predict phase relations, and to define processing conditions for multicomponent alloys. Investigations carried out in our group have contributed to better description of phase diagrams for several binaries systems[1–6]. Based on inconsistencies between the most recent assessments[7,8] as well as data from heat-treated ternary alloys[8–11] containing Nb and Al, new investigations on the solubility limits of the intermetallic phases of the Nb-Al system are necessary. Thus, in this work, the solubility limits of the (Nb), Nb_3Al, Nb_2Al and the Nb-rich side of the $NbAl_3$ phase were reevaluated via Electron Probe Microanalysis – Wavelength dispersive spectrometry (EPMA – WDS) from equilibrated alloys.

2. Literature Review

Table 1 summarizes the experimental information available for the Nb-Al system concerning *solidus/liquidus* temperatures, phase solubility range, activity data and enthalpy of formation.

2.1 Phase equilibria data

Due to its importance for the development of superconductors and high-temperature materials, many authors have investigated the Nb-Al phase diagram. The early studies of this system[12–19] are all in relatively good agreement in terms of phase stability. Besides the terminal compounds, the Nb_3Al (A15), Nb_2Al (σ) and $NbAl_3$ ($D0_{22}$) phases are reported as stable (see Table 2 for crystallographic structural information), however, Richards [15] indicates the presence of 2 extra high temperature phases (Nb_7Al_3 and $Nb_{17}Al_3$) which have not been reported by other authors. The congruent formation of $NbAl_3$ is well established, however, there have been some discrepancies in terms of the nature of formation of the other phases. For example, Nb_3Al is reported to be formed either peritectoidically[15,17] or peritectically[14,16,19], while Nb_2Al is reported to be formed either congruently[15,19] or peritectically[14,16,17]. The Al-rich side of this system is characterized by a degenerated equilibrium in which the Liquid, $NbAl_3$ and (Al) phases are involved. This invariant reaction has been reported either as eutectic [14,15] or peritectic [12,13,16].

The most complete experimental work on the Nb-Al system was carried out by Jorda et al.[20]. In this paper, the authors determined the phases' solubilities ranges via metallography, XRD and EPMA analysis of samples heat-treated from 24 hours up to 1 month according to the temperature of heat treatment. The authors also used levitation thermal analysis (LTA) and differential thermal analysis (DTA) to determine the temperature of the invariant reactions, *solidus* and *liquidus*, and the peritectic nature for the Nb_3Al and Nb_2Al formation

*e-mail: aaaps@unifei.edu.br

Table 1. Summary of Experimental information available for the Nb-Al System.

Information	Reference	Technique
Temperatures (*Solidus/Liquidus*)	Jorda et al.[20]	DTA/LTA
	Stein et al.[25]	DTA
	Wicker et al.[18]	DTA
	Witusiewicz et al.[7]	DTA/PA
	Zhu et al.[24]	DSC
	Lundin and Yamamoto[16]	DTA
	Baron and Savitskii[14]	TA
	Svechnikov et al.[17]	TA
Phase solubility Range	This work	EPMA
	Menon et al.[22]	EPMA
	Kokot et al.[21]	XRD
	Shilo et al.[23]	Knudsen Effusion
	Jorda et al.[20]	EPMA
		MA
		XRD
	Lundin and Yamamoto[16 (a)]	MA
		Hardness
		XRD
	Svechnikov et al.[17(a)]	XRD
	Glazov et al.[12,13]	Hardness[(b)]
Enthalpy of Formation of Intermetallic Phases	Colinet et al.[27]	LMTO-FP
	De Boer et al.[28]	Miedema Model
	Meschel et al.[29]	DRC
	Shilo et al.[23]	Knudsen Effusion
	George et al.[31]	EMF
	Mahdouk et al.[30]	DRC

(a) apud Jorda et al.[20]; (b) Solubility of Nb in (Al); DTA: Differential Thermal Analysis; LTA: Levitation Thermal Analysis; PA: Pirani-Alterthum Method; TA: Thermal Analysis; DSC: Differential Scanning Calorimetry; EPMA: Electron Probe Microanalysis; XRD: X-ray Diffractometry; MA: Metallographic Analysis; LMTO: full potential Linear Muffin tin orbital; DRC: Direct Reaction Calorimetry; EMF: Electromotive Force.

Table 2. Crystallographic information of stable solid phases of the Nb-Al system[40].

Phase	Strukturbericht Designation	Pearson Symbol	Space Group	Prototype	Occupation	Wyckoff	x	y	z
(Nb)	A2	cI2	$Im\bar{3}m$	W	Nb	2a	0	0	0
Nb_3Al	A15	cP8	$Pm\bar{3}n$	Cr_3Si	Al (1)	2a	0	0	0
					Nb (1)	6c	0.25	0	0.5
Nb_2Al	$D8_b$	tP30	P42/mnm	CrFe	Al (1)	2a	0	0	0
					Al (2)	8i	0.0665	0.2615	0
					Nb (1)	8i	0.535	0.128	0
					Nb (2)	4g	0.3965	0.6035	0
					Nb (3)	8j	0.318	0.318	0.252
$NbAl_3$	$D0_{22}$	tI8	I4/mmm	$TiAl_3$	Al (1)	2b	0	0	0.5
					Al (2)	4d	0	0.5	0.25
					Nb (1)	2a	0	0	0
(Al)	A1	cF4	$Fm\bar{3}m$	Cu	Al	2a	0	0	0

was confirmed. The solubility limits of the phases were also indirectly determined by Kokot et al. [21] via XRD analysis of arc-melted samples heat-treated for 14 days at 1100 °C and Menon et al. [22] via EPMA measurements of arc-melted alloys heat-treated at 1650 °C/50 h and subsequently heat treated at 1200 °C/14 days or 1000 °C/30 days. Shilo et al. [23] measured the variation of vapor pressure of Al according to the composition from binary alloys and indirectly determined the solubility limits of the phases. Their samples were previously heat-treated at 1297 °C for 12 hours and then the vapor pressures were measured at 1571, 1607, 1672, 1721 °C with different times and heating/cooling cycles.

Zhu et al. [24] performed Differential Scanning Calorimetry (DSC) measurements with different scanning rates from heat treated samples in order to determine the nature of the Al-rich equilibrium involving Liquid, $NbAl_3$ and (Al). The suggested temperature was 661.44 °C, leading to a peritectic type reaction because it is higher than the melting point of pure Al (660.3 °C). Witusiewicz et al. [7] performed new experiments (DTA and Pirani-Alterthum method) aiming at the determination of the high temperature *solidus* and *liquidus* lines. In general, their results are in good agreement with previous information [20]. Witusiewicz et al. [7] also measured the temperature of the degenerated Al-rich reaction as 657 °C ± 5 (DTA), despite this, they modeled the reaction as peritectic. More recently, Stein et al. [25] measured the $NbAl_3$ ($D0_{22}$) phase congruent melting temperature via DTA.

2.2 Thermodynamic data and CALPHAD modeling

Several studies present estimated data for enthalpies of formation of the Nb-Al compounds based both in calculations as well as on experimental results. Gelashvili and Dzneladze [26] estimated the enthalpies of formation calculating the changes in the free energy of the process of reduction of Al and Nb oxides with CaH_2. Colinet et al. [27] reported the enthalpies of formation of the intermetallic phases via first principle calculations (Full Potential Linear Muffin Tin Orbital, FP-LMTO) and de Boer et al. [28] via Miedema Model. Shilo et al. [23] carried out vapor pressure measurements in the high-temperature range 1844-2146 K using the Knudsen Effusion Method aiming the determination of enthalpy of formation of the intermetallic compounds. Meschel and Kleppa [29] and Mahdouk et al.[30] conducted experiments of Direct Reaction Calorimetry (DRC). George et al. [34] performed Electromotive Force (EMF) measurements in the intermediate temperature (973 to 1078 K) range by using solid-state electrochemical cells and CaF_2 as solid electrolyte. George et al. [31] and Shilo et al.[23] also have measured the activities of Al in the Nb-Al system.

The Nb-Al system was firstly described according to the CALPHAD methodology by Kaufman and Nesor [32], considering all compounds as stoichiometric. Latter, it was reassessed by Kaufman [33] where the Nb_2Al phase was modeled as a substitutional solid solution. Subsequent studies have modeled the Nb_3Al phase either as $(Nb)_3(Al,Nb)_1$ [8,24,34,35] or $(Al,Nb)_3(Al,Nb)_1$ [7,36], the Nb_2Al phase mostly as $(Al,Nb)_5(Nb)_2(Nb,Al)_8$ and the $NbAl_3$ phase has been modeled as either stoichiometric [24,34] or $(Al,Nb)_1(Al,Nb)_3$ [7,8,35,36]. Joubert [37] investigated the Nb_2Al site occupancy via Rietveld refinement of X-ray diffraction data and Mathieu et al. [38] investigated simplifications for the σ phase sublattice models, evaluating the best agreement with the experimental phase diagram. The model type $(Al,Nb)_2(Al,Nb)_8(Al,Nb)_5$ should be used in order to respect the crystal structure and the nature of the defects in this phase. Table 3 summarizes the sublattices models applied for the description of these intermetallic phases from assessments of different authors.

3. Experiments Procedure

Alloys with initial masses between 1 and 2 g were weighed on an analytical balance with accuracy of 0.1 mg from high purity raw materials, Al (min. 99.999 wt. %) and Nb (min. 99.8 wt. %)

3.1 Arc-melting

The alloys were arc-melted in a water-cooled copper crucible under argon atmosphere (min. 99.995%) and non-consumable tungsten electrode. Five melting steps were carried out for each alloy to ensure chemical homogeneity, turning the ingots upside-down from one melting step to the next. Before each melting step a piece of pure Ti (getter) was melted to remove residual gas impurities from the furnace atmosphere. After melting, the ingots were weighed to evaluate possible mass losses during arc-melting.

Table 3. Sublattice models used for the Nb-Al phases in literature CALPHAD assessments of the Nb-Al system.

Reference	Sublattice model		
	Nb_3Al (A15)	Nb_2Al (σ)	$NbAl_3$ ($D0_{22}$)
He et al.[8]	$(Nb)_3(Al,Nb)_1$	$(Al,Nb)_5(Nb)_2(Nb,Al)_8$	$(Al,Nb)_1(Al,Nb)_3$
Witusiewicz et al.[7]	$(Al,Nb)_3(Al,Nb)_1$	$(Al,Nb)_5(Nb)_2(Nb,Al)_8$	$(Al,Nb)_1(Al,Nb)_3$
Zhu et al.[24]	$(Nb)_3(Al,Nb)_1$	$(Al,Nb)_5(Nb)_2(Nb,Al)_8$	Stoichiometric
Shao[34]	$(Nb)_3(Al,Nb)_1$	$(Al)_{0.267}(Nb)_{0.133}(Al,Nb)_{0.6}$	Stoichiometric
Servant and Ansara[36]	$(Al,Nb)_3(Al,Nb)_1$	$(Al,Nb)_5(Nb)_2(Nb,Al)_8$	$(Al,Nb)_1(Al,Nb)_3$
Kattner and Boettinger[35]	$(Nb)_3(Al,Nb)_1$	$(Al,Nb)_5(Nb)_2(Nb,Al)_8$	$(Al,Nb)_1(Al,Nb)_3$
Kaufman[33]	Stoichiometric	(Al,Nb)	Stoichiometric
Kaufman and Nesor[32]	Stoichiometric	Stoichiometric	Stoichiometric

3.2 Heat treatments

Aiming to reach thermodynamic equilibrium conditions, all alloys where heat treated at 1400 °C for 75 h in a resistive (Ta heating element) furnace under argon. The temperature was measured by an optical pyrometer calibrated against the melting point of pure elements. Subsequently, samples of each alloy were wrapped in thin Ta foil, encapsulated in quartz tubes (under argon) and heat treated at 1200 °C for 200 h or 1000 °C for 600 h using tubular resistive furnaces.

3.3 X-ray diffractometry (XRD)

For the X-ray diffraction experiments, the samples were analyzed in powder form, with powder size below 80 mesh (178 µm). The following conditions were adopted: Cu-Kα radiation, 40 kV voltage, 30 mA current, 0.02º angular step, 15s per step, and angle (2θ) ranging from 10 to 90°. The phases present in the samples were identified by comparison between experimental and simulated diffractograms, using PowderCell Software[39] with crystallographic information reported by Villars and Calvert[40]. The lattice parameters for the Nb_2Al phase were obtained via Rietveld refinement using the software FullProf[41].

3.4 Scanning electron microscopy and electron probe micro-analysis

The samples were prepared according to the following route: (1) hot mounting; (2) manual grinding with SiC sand paper, in the sequence: 220, 400, 600, 1200, 2400, 4000; (3) Final polishing with a colloidal silica suspension (OP-S); (4) ultrasonic cleaning for 15 minutes; (5) coating with carbon. Initial images were obtained in the backscattered electron mode in conventional SEM microscopes (TM3000, Hitachi), equipped with Energy Dispersive Spectrometers (EDS). The determination of alloys' global composition was made via EDS measurement in representative area (at least 0.15 mm^2) skipping possible cracks and pores. Wavelength X-ray Spectroscopy (WDS) analyses were performed in a SX100 (CAMECA) instrument equipped with 5 spectrometers. The standards were Pure Nb (min. 99.8 wt.%) and Pure Al (min. 99.999 wt.%). The compositions proposed for the phases are the average values of at least 7 measurements in different regions of the sample.

4. Results and Discussion

4.1 Solubility range

Table 4 shows the chemical composition of the prepared alloys, the mass losses associated with the melting steps, and the calculated composition interval for each alloy assuming that all mass losses were either from Nb or Al volatilization. Alloy Nb60Al presented an important mass variation, however, EDS analysis indicated that the global composition of the sample was kept. Thus, it should have occurred due to macroscopic pieces of the alloy that were thrown out of the crucible during cooling inside the arc-melter.

Table 4. Compositions of the Nb-Al alloys prepared in this work, after arc-melting.

Alloy Id	Composition (at.% Al)	Mass Variation (%)	Possible Composition Interval* (at.% Al)	
			a	b
Nb12Al	12.0	0.92	9.4	12.1
Nb23Al	25.1	0.87	23.1	25.2
Nb60Al	59.9	7.33	53.1	62.5

*calculated composition attributing mass loss to either (a) Al or (b) Nb.

Figure 1 presents the X-ray diffractograms of the alloys equilibrated at 1000, 1200 and 1400 °C. All peaks were identified and only the expected phases are present in the alloys: (Nb) + Nb_3Al (Nb12Al); Nb_3Al + Nb_2Al (Nb23Al); Nb_2Al+$NbAl_3$ (Nb60Al).

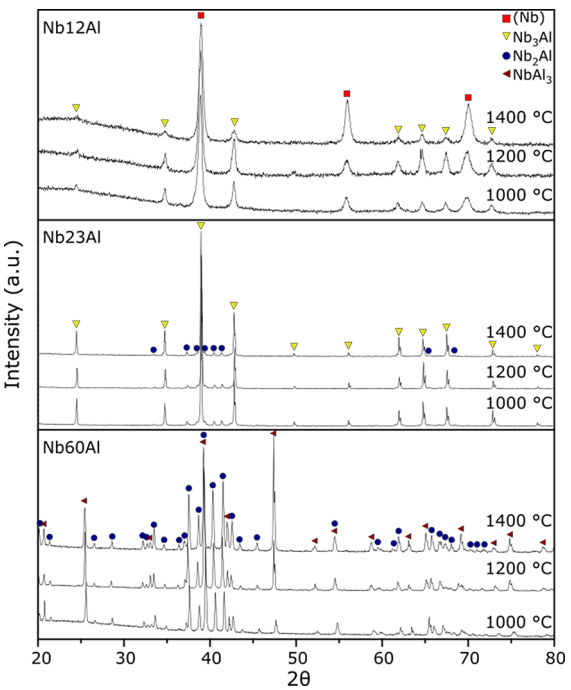

Figure 1. X-ray diffractograms of the Alloys: [a] Nb12Al, [b] Nb23Al and [c] Nb60Al equilibrated at 1000, 1200 and 1400 °C.

Figure 2 presents SEM micrographs of the heat-treated alloys, with significant microstructural differences from the as-cast condition, indicating that significant diffusion process occurred, and the equilibria was achieved. Alloy Nb12Al in all conditions presented grains of (Nb) and intergranular Nb_3Al. In the interior of the (Nb) grains, precipitates of Nb_3Al are observed in the samples equilibrated at 1000 and 1200 °C, but not in the sample equilibrated at 1400 °C. The formation of

these precipitates is due a solid state precipitation of Nb_3Al that came from a supersaturated (Nb). No significant change is observed in the microstructures of the Alloy Nb23Al with the heat treatment conditions. These samples show Nb_3Al matrix and a fraction of distributed Nb_2Al. Micrographs of Alloy Nb60Al present a microstructure with alternate plates of Nb_2Al and $NbAl_3$.

Table 5 shows the composition of the alloys measured via EDS and the phases measured via EPMA along with the error which is calculated based on the standard deviation of the measured values. The presence of precipitates in the interior of the (Nb) phase equilibrated at 1000 °C did not allowed reliable EMPA measurements. Results of EPMA measurements are also plotted in Figure 3 along with selected experimental data available in the literature as well as the calculated phase diagrams with the parameters optimized by Witusiewicz et al. [7] and He et al. [8]. The measurements in the (Nb), Nb_3Al and $NbAl_3$ phases are in agreement with the literature experimental data as well as the Nb-rich limit of the Nb_2Al phase. The Al-rich limit of the Nb_2Al phase exhibits important discrepancies with the most recent assessment.

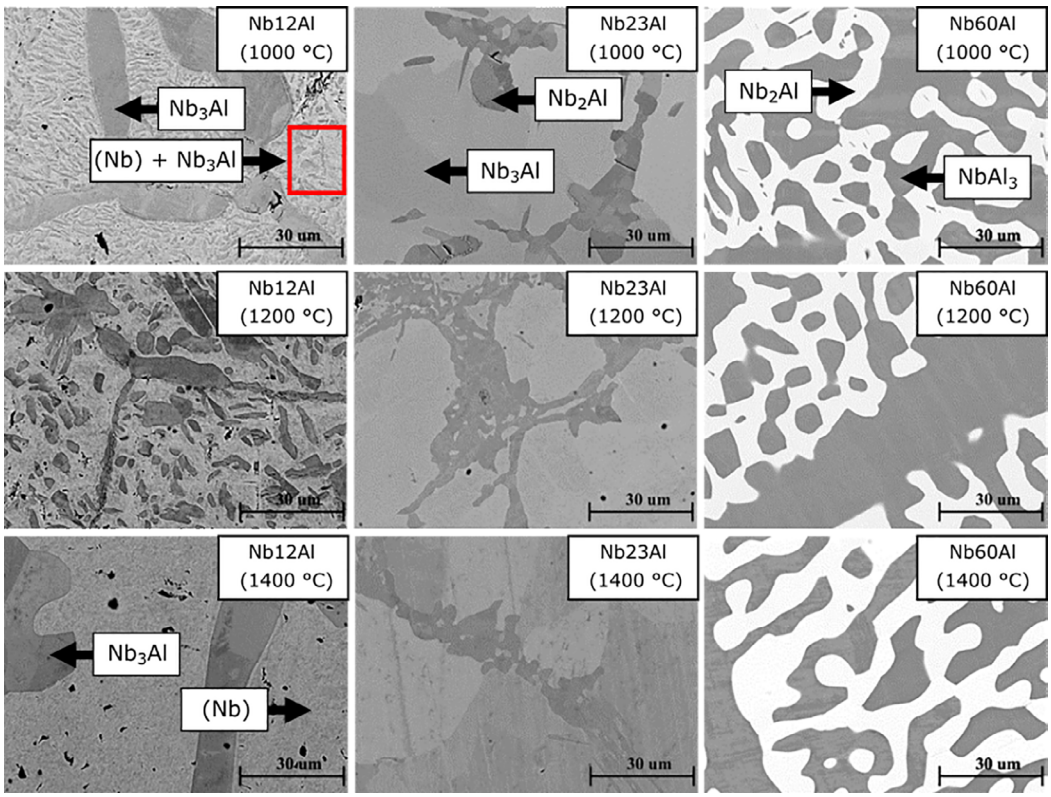

Figure 2. Evolution of the microstructure of the Alloys Nb12Al, Nb23Al and Nb60Al equilibrated at 1000, 1200 and 1400 °C.

Table 5. Composition limits of the phases of the Nb-Al system measured via EPMA.

Alloy	Equilibrated Temperature (°C)	Global Composition - EDS (at. % Al)	Phase Composition - EPMA (at. % Al)	
			(Nb)	Nb_3Al (A15)
Nb12Al	1400	10.3	-	19.3 ± 0.2
	1200	11.3	6.5 ± 0.7	18.6 ± 0.4
	1000	11.1	7.1 ± 1.1	19.3 ± 0.6
			Nb_3Al (A15)	Nb_2Al (σ)
Nb23Al	1400	21.9	23.1 ± 0.2	31.5 ± 0.3
	1200	21.7	23.0 ± 0.1	31.7 ± 0.1
	1000	21.6	23.2 ± 0.1	31.9 ± 0.2
			Nb_2Al (σ)	$NbAl_3$ ($D0_{22}$)
Nb60Al	1400	57.7	42.4 ± 0.2	74.4 ± 0.1
	1200	58.7	39.4 ± 0.6	74.8 ± 0.3
	1000	59.3	36.7 ± 0.9	74.7 ± 0.1

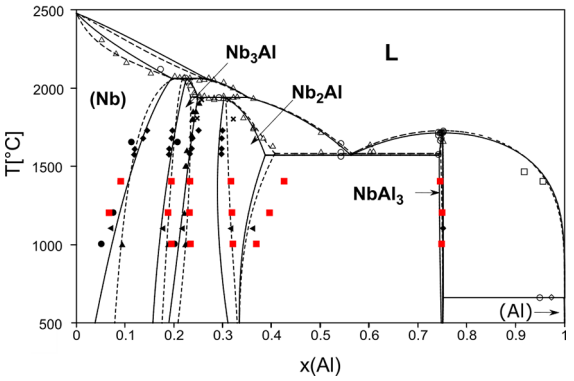

Figure 3. Nb-Al phase diagram calculated with the parameters optimized by Witusiewicz et al.[7] (solid lines) and He et al.[8] (dashed lines) along with experimental data from: This work (■ EPMA), Jorda et al.[20] (▲ XRD; Δ DTA/LTA; × EPMA), Kokot et al. [21] (◄ XRD), Menon et al.[22] (● EPMA), Shilo et al.[23] (♦ Knudsen Effusion), Witusiewicz et al.[7] (○ DTA), Wicker et al.[18] (□ DTA) and Zhu et al.[24] (◊ DSC). Note: (Nb) phase's composition measurement in Nb12Al alloy equilibrated at 1000 °C was removed from the figure because of its low reliability.

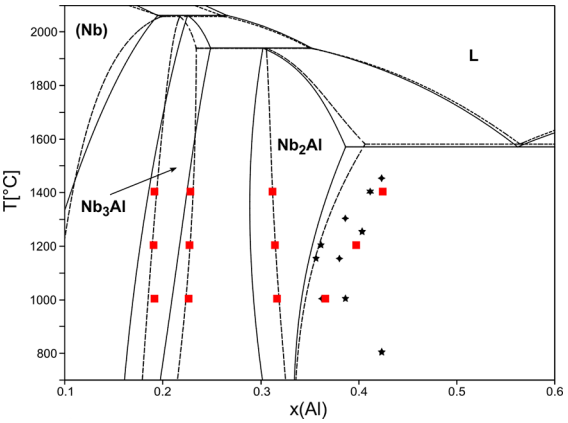

Figure 4. Details of Nb-Al phase diagram calculated with the parameters optimized by Witusiewicz et al.[7] (solid lines) and He et al.[8] (dashed lines) along with experimental data from: This work (■ EPMA), ternary Co-Nb-Al ★ [11] and Fe-Nb-Al ✦ [9], ✸ [10] alloys.

Figure 4 show details of the Nb-Al phase diagram in the Nb_2Al region along with the EPMA composition measurements for this phase. The square symbols are from the present work while the stars are from measurements in ternary samples (Al-Co-Nb [11] or Al-Fe-Nb [9,10]) positioned in three phase field equilibria in which the third component (Co or Fe) solubility is lower than 1 at.% in the Nb_2Al phase. Our results are in agreement with the results from Silva [10] (alloy heat treated at 1400 °C/75h) and Stein et al. [9] (alloys heat treated at 1450 °C/50 h, 1150 °C /168 h and 1000 °C/1000 h). However, the alloy heat treated at 1300 °C/100 h in the work of Stein et al. [9] presented a slightly lower Al solubility. Compared with the results from Dovbenko et al. [11], our results are in agreement with the measurement obtained from the alloy heat treated at 1250 °C/72 h. However, the results at 1200 °C/96 h and 1150 °C/136 h presented significantly lower Al contents while for the samples 1000 °C/236 h and 800 °C/1000 h the contents were higher than the expected.

4.2 XRD rietveld refinement

Figure 5 shows the lattice parameters "a" and "c" for the Nb_2Al phase in function of temperature, along with the results from Kokot et al. [21] and Joubert [37]. The symbols in black (◄and ■) represent the parameters obtained for the Nb-rich side of the Nb_2Al phase (results from alloys in Nb_3Al+Nb_2Al field), while the gray symbols (◄and■) the parameters obtained for the Al-rich side of the phase (results from alloys in Nb_2Al+$NbAl_3$ field). It should be stated that Joubert [37] results (symbol ●) is from a Nb_2Al single phase alloy with composition 34.2 at.% of Al. In general, our results are in agreement with Kokot et al. [21] as well as results from Joubert [37]. The presence of excess Al in the structure of Nb_2Al promoted the decreasing of the parameter "a" and increasing of the parameter "c" of the crystal structure. This can be noted both in a fixed temperature, comparing the Al-rich side with the Nb-rich side as well as the lattices parameters change when the solubility of Al increases with the temperature (Al-rich side).

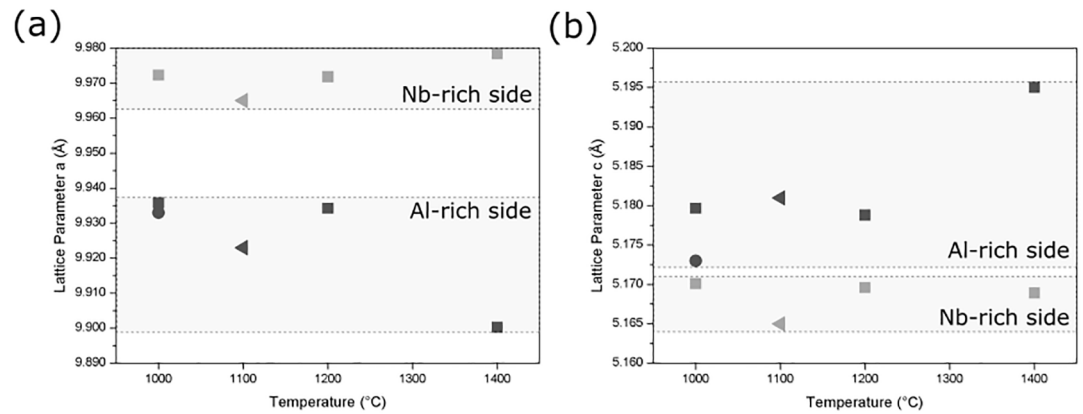

Figure 5. Lattice parameters [a] "a" and [b] "c" for the Nb2Al phase as a function of the heat treatment temperature. Symbols are from Kokot et al.[21] (◄), Joubert[37] (●) and this work (■).

5. Conclusions

Experiments aiming to determine the solubility limits of the intermetallic phases in the Nb-Al system confirmed the solubility range for the phases (Nb) and Nb_3Al. The Nb-rich sides of the phases $NbAl_3$, Nb_2Al were also in agreement with the previous data. Different values from those reported in the literature were found for the Al-rich border of the Nb_2Al phase. The present experimental results are consistent with the experimental data in the ternary alloy systems containing Nb and Al [8–11], suggesting necessary changes in the currently accepted Nb-Al phase diagram and the thermodynamic description of this system, specially concerning the Nb_2Al phase.

6. Acknowledgements

This work is based upon financial support by CAPES/COFECUB (665/10) and CNPq (140069/2013-5), to which the authors gratefully acknowledge.

7. References

1. Silva AAAP, Ramos ECT, Faria MIST, Coelho GC, Nunes CA. The Ta-Si System: Reevaluation of the Liquid Compositions in the Invariant Reactions and Determination of the Invariant Reaction Involving Both βTa5Si3 and αTa5Si3 Phases. *Journal of Phase Equilibria and Diffusion*. 2015;36(3):209-217.

2. Gigolotti JCJ, Nunes CA, Suzuki PA, Coelho GC. Evaluation of Phase Equilibria Involving the Liquid Phase in the Hf-Si System. *Journal of Phase Equilibria and Diffusion*. 2014;35(5):622-630.

3. Gigolotti JCJ, Chad VM, Faria MIST, Coelho GC, Nunes CA, Suzuki PA. Microstructural characterization of as-cast Cr–B alloys. *Materials Characterization*. 2008;59(47):74-78.

4. Baldan R, Faria MIST, Nunes CA, Coelho GC, Chad VM, Avillez RR. Microstructural Evidence of βCo2Si-phase Stability in the Co-Si System. *Journal of Phase Equilibria and Diffusion*. 2008;29(6):477-481.

5. Nunes CA, Coelho GC, Ramos AS. On the invariant reactions in the Mo-rich portion of the Mo-Si system. *Journal of Phase Equilibria and Diffusion*. 2001;22(5):556-559.

6. Silva AAAP, Ferreira F, Lima-Kühn BB, Coelho GC, Nunes CA, Vilasi P, et al. The Ta-B system: Key experiments and thermodynamic modeling. *Calphad-Computer Coupling Of Phase Diagrams And Thermochemistry*. 2018;63:107-115.

7. Witusiewicz VT, Bondar AA, Hecht U, Rex S, Velikanova TY. The Al–B–Nb–Ti system: III. Thermodynamic re-evaluation of the constituent binary system Al–Ti. *Journal of Alloys and Compounds*. 2008;465(1-2):64-77.

8. He C, Stein F, Palm M. Thermodynamic description of the systems Co–Nb, Al–Nb and Co–Al–Nb. *Journal of Alloys and Compounds*. 2015;637:361-375.

9. Stein F, He C, Prymak O, Voß S, Wossack I. Phase equilibria in the Fe–Al–Nb system: Solidification behaviour, liquidus surface and isothermal sections. *Intermetallics*. 2015;59:43-58.

10. Silva AAAP. Thermodynamic modeling and critical experiments on the Al-Fe-Nb system [Thesis]. São Paulo: São Paulo University (USP); 2015.

11. Dovbenko O, Stein F, Palm M, Prymak O. Experimental Determination of the Ternary Co–Al–Nb Phase Diagram. *Intermetallics*. 2010;18(11):2191-2207.

12. Glazov VM, Vigdorovich VN, Korolkov GA. Issledovanie vzaimodeistviya alyuminiyas niobium. *Zhurnal Neorganicheskoi Khimii*. 1959;4:1620-1624.

13. Glazov VM, Lazarev GP, Korolkov GA. The solubility of certain transition metals in aluminum. *Metal Science and Heat Treatment*. 1959;1(10):51-53.

14. Baron VV, Savitskii EM. Diagramma sostoyaniya niobiy–alyuminiy. *Zhurnal Neorganicheskoi Khimii*. 1961;6:182-185.

15. Richards MJ. Contribution a l'étude du système niobium/aluminium. *Journées Métallurgiques d'Automne Paris* (1962) 1-12.

16. Lundin C, Yamamoto A. Equilibrium Phase Diagram, Niobium (Columbium)-Aluminum. *Transactions of the Metallurgical Society of AIME*. 1966;236:863-872.

17. Svechnikov VN, Pan VM, Latysheva VI. Phase diagram of niobium-aluminum system. *Metallofizika*. 1968;22:54-61.

18. Wicker A, Allibert C, Droile J. Contribution on the study of the NbAl3-Al phase diagram. *Comptes Rendus l'Académie Des Sciences*. 1971;272C:1711-1713.

19. English JJ. Binary and ternary phase diagrams of columbium, molybdenum, tantalum, and tungsten (Report). *Def. Met. Inf. Cent.* 1963.

20. Jorda JL, Flukiger R, Muller J. A New metallurgical investigation of the niobium-aluminium system. *Journal of Less Common Metals*. 1980;75(2):227-239.

21. Kokot L, Horyn R, Iliew N. Niobium – Aluminum binary system phase equilibria at 100 °C and superconductivity of alloys. *Journal of Less Common Metals*. 1976;44:215-219.

22. Menon ESK, Subramanian PR, Dimiduk DM. Phase Equilibria in Nb-rich Nb-Al-Ti Alloys. *Scripta Metallurgica et Materialia*. 1992;27(3):265-270.

23. Shilo I, Franzen HF, Schiffman RA. Enthalpies of Formation of Niobium Aluminides as Determined by the Knudsen Effusion Method. *Journal of the Electrochemical Society*. 1982;129(7):1608-1613.

24. Zhu Z, Du Y, Zhang L, Chen H, Xu H, Tang C. Experimental identification of the degenerated equilibrium and thermodynamic modeling in the Al–Nb system. *Journal of Alloys and Compounds*. 2008;460(1-2):632-638.

25. Stein F, He C, Wossack I. The liquidus surface of the Cr–Al–Nb system and re-investigation of the Cr–Nb and Al–Cr phase diagrams. *Journal of Alloys and Compounds*. 2014;598:253-265.

26. Gelashvili GA, Dzneladze ZI. Thermodynamic calculation of the reactions occurring in the preparation of the intermetallic compound Nb3Al by the method of simultaneous reduction of niobium and aluminum oxides with calcium hydride. *Poroshkovaya Metalurgyl*. 1979;8:13-16.

27. Colinet C, Pasturel A, Manh DN, Pettifor D, Miodownik P. Phase stability of the Al-Nb system. *Physical Review: B*. 1997;56:552-565.

28. Boer FR, Boom R, Mattens WCM, Miedema AR. *Cohesion in Metals: Transition Metal alloys*. Amsterdam: North Holland; 1989.

29. Meschel SV, Kleppa OJ. Standard enthalpies of formation of 4d aluminides by direct synthesis calorimetry. *Journal of Alloys and Compounds*. 1993;191:111-116.

30. Mahdouk K, Gachon JC, Bouirden L. Enthalpies of formation of the Al-Nb intermetallic compounds. *Journal of Alloys and Compounds*. 1998;268(2):118-121.

31. George P, Parida SC, Reddy RG. Thermodynamic Studies of Nb-Al System. *Metallurgical and Materials Transactions: B.* 2007;38(1):85-91.

32. Kaufman L, Nesor H. Coupled phase diagrams and thermochemical data for transition metal binary systems — V. *Calphad*. 1978;2(4):325-348.

33. Kaufman L. Calculation of multicomponent tantalum based phase diagrams. *Calphad*. 1991;15(3):251-282.

34. Shao G. Thermodynamic assessment of the Nb–Si–Al system. *Intermetallics*. 2004;12:655-664.

35. Kattner UR, Boettinger WJ. Thermodynamic calculation of the ternary Ti−Al−Nb system. *Materials Science and Engineering: A*. 1992;152:9-17.

36. Servant C, Ansara I. Thermodynamic assessment of the Al-Nb system. *The Journal of Chemical Physics*. 1997;94:869-888.

37. Joubert JM. Crystal chemistry and Calphad modeling of the composition may be significantly weaker. the sigma phase. *Progress in Materials Science*. 2008;53:528-583.

38. Mathieu R, Dupin N, Crivello JC, Yaqoob K, Breidi A, Fiorani JM, et al. CALPHAD description of the Mo–Re system focused on the sigma phase modeling. *Calphad*. 2013;43:18-31.

39. Kraus W, Nolze G. *PowderCell for Windows (version 2.3)*. Berlin: Federal Institute for Materials, Research and Testing; 1999.

40. Villars P, Calvert LD. *Pearson's handbook of crystallographic data for intermetallic phases*. 2nd ed. Materials Park, OH: ASM International; 1991.

41. Platas J, Carvajal JR. *FullProf2000 and WinPLOTR - Applications for Diffraction Commission For Powder Diffraction*. Chester: International Union for Crystallography; 2000.